Water Practice & Technology

IWA PUBLISHING

Water Practice & Technology Vol 17 No 1, 502 doi: 10.2166/wpt.2021.129

Bentonite blended with bagasse ash as an adsorbent for reactive red 198 dyes

Teshale Adane[a], Amare Tiruneh Adugna[a,b] and Esayas Alemayehu[c,d,*]

[a] Department of Environmental Engineering, Addis Ababa Science and Technology University, Addis Ababa, P.O. Box 16417, Ethiopia
[b] Bioprocess and Biotechnology Center of Excellence, Addis Ababa Science and Technology University, Addis Ababa, P.O. Box 16417, Ethiopia
[c] Faculty of Civil and Environmental Engineering, Jimma University, Jimma, P.O. Box 378, Ethiopia
[d] Africa Center of Excellence for Water Management, Addis Ababa University, Addis Ababa, P.O. Box 1176, Ethiopia
*Corresponding author. E-mail: esayas16@yahoo.com

ABSTRACT

Adsorption offers an efficient, cost-effective, and eco-friendly method for the treatment of dye-laden wastewater. This work presents reactive red 198 (RR198) removal by adsorption using bentonite clay (BC) blended with sugar cane bagasse ash (SCBA). The adsorbent's surface morphologies, crystalline phase structures, functional groups, and specific surface before and after adsorption were examined using SEM, XRD, FTIR, and BET respectively. Central composite design (CCD) under response surface methodology (RSM) was applied to optimize independent and dependent variable values. The optimal parameters for RR198 removal using the blended adsorbent were 107 minutes contact time, 0.934 g/L adsorbent dose, and 15 mg/L initial dye concentration, and 85.2% RR198 removal efficiency was achieved. The sorption isotherms and kinetics were evaluated using various existing models. The Freundlich isotherm model ($R^2 = 0.95$) and the pseudo-second-order equation best described the adsorption parameters and the RR198 adsorption kinetic mechanism, respectively. Desorption and reusability experiments in batch study confirmed that BC blended with SCBA can be used multiple times for dye removal from wastewater.

Key words: adsorption, blended low-cost adsorbent, reactive red 198 dyes, response surface methodology

HIGHLIGHTS

- Bentonite blended with SCBA as adsorbent removed RR198 from synthetic solution successfully.
- The highest RR 198 removal efficiency from water was at pH 2.
- CCD under RSM was applied to determine optimal parameters of independent and dependent variables.

GRAPHICAL ABSTRACT

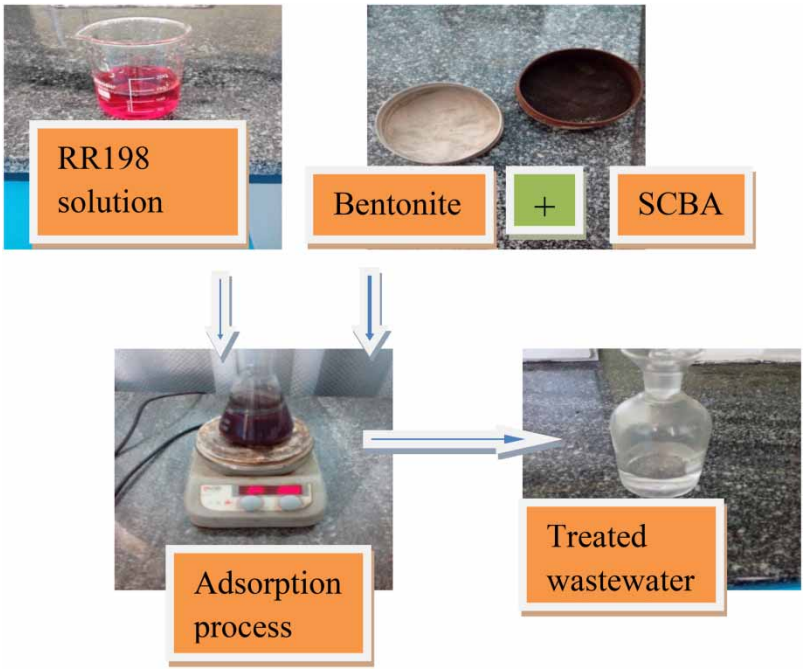

1. INTRODUCTION

Dye-laden industrial effluents bring several environmental challenges with them. Both reactive and basic dyes are consumed in the textile, paper, plastic, and other industries as coloring agents. The textile industry, uses about 56% of total annual synthetic dye production worldwide (Jain & Gogate 2018). Because of incomplete binding onto materials and inadequate control, huge volumes of dyes are discharged into the environment in untreated wastewater, leading to serious health and environment issues.

Dyes are harmful to living organisms due to their recalcitrant and non-biodegradable properties (Moussavi & Khosravi 2011). Aquatic organisms and humans can be affected by carcinogenic and teratogenic effects of dye (Song *et al.* 2017). Dyes can also affect various human organs including the kidney, liver, and nervous system (Zhou *et al.* 2015). Discharge of wastewater containing dyes into water bodies reduces the photosynthetic activity of aquatic plants and, in turn, the natural equilibrium.

The binding rates of reactive dyes onto material fibers are estimated to be between 60 and 70%, so that about 40% of that used is released into the environment (Alimohammadi *et al.* 2016). Dyes are water soluble and inhibit light transmission through water, and cannot be removed easily using conventional treatment techniques. Reactive dye-laden effluents are toxic and mutagenic, and enhance water body hazards as well as being difficult to remove by biological treatment. Thus, it is necessary to design efficient wastewater treatment technologies for dye removal or remediation before effluents are released into the environment. Known technologies including the advanced oxidation process, ion exchange, microbial fuel cells, ozonation, coagulation, flocculation, and adsorption have been applied to remediate or remove different dyes from industrial effluents (Adebayo *et al.* 2020). The limitations of these technologies include cost, fouling issues, regular maintenance, and complicated operational procedures (Garg *et al.* 2003; Dizge *et al.* 2008).

Adsorption is still one of the most widely used dye treatment methods, taking the lead in high removal efficiency, operating simplicity, low operating cost, eco-friendliness, and the availability of a large variety of adsorbents (Gupta *et al.* 2004; Khalilzadeh Shirazi *et al.* 2020). Commercial activated carbon is commonly used as an adsorbent for dye removal from wastewater due to its adsorptive efficiency and capacity. Its high associated cost and difficulty in regeneration offer disadvantages (Srivastava *et al.* 2007). Various adsorbents have been investigated in their natural form for dye removal from wastewater including bagasse fly ash (Mall *et al.* 2005), bentonite/charred dolomite (Khalilzadeh Shirazi *et al.* 2020), natural bentonite (Carvalho *et al.* 2019), fly ash (Dizge *et al.* 2008), and pine cone (Dawood & Sen 2012). Many of these suffer from long synthesis

procedures, however, or short lifespans making their use impractical in many parts of the world. Consequently, efforts have been made to obtain easily accessible and efficient adsorbents that can be used to treat dye-laden wastewaters in low-income countries such as Ethiopia.

Adsorption can be enhanced by blending with bio-waste materials, which enhance or increase an adsorbent mineral's capacity. Sugar cane bagasse ash (SCBA) is used in landfill and has negligible value (Huabcharoen *et al.* 2017) but creates environmental and human health problems when handled improperly and disposed into the soil, air or water (Farirai *et al.* 2020). Thus, agricultural wastes used as adsorbent reduce solid waste volumes and follow the principle of generating money from waste.

Little experimental data or literature are available on reactive dye removal – e.g. reactive red 198 (RR198) – using bentonite blended with SCBA. Bentonite is widely available and with its dye adsorption capacity (Pandey & Ramontja 2016) can be used as a low-cost dye removal adsorbent (Toor *et al*. 2015; Carvalho *et al.* 2019).

In this study, adsorption experiments were carried out to investigate the application of a novel blended adsorbent system – bentonite and SCBA – for reactive dye sorption.

2. MATERIALS AND METHODS

2.1. Adsorbents and Adsorbate

Bentonite and SCBA were collected from *Gewane* (Afar region) and *Wonji Shewa* sugar factory (Oromia region), Ethiopia, respectively. The bentonite was crushed, washed using distilled water, dried in an oven (FAITHFUL) at 105 °C for 12 hours, and ground to a powder. The latter was screened in a sieve shaker to 125 μm particle size. The SCBA was also washed using distilled water and dried in an oven (FAITHFUL) at 105 °C for 12 hours before screening to 125 μm particle size. The adsorbent materials were stored in glass bottles. The RR198 dye was obtained from the *Yirgalem* Addis textile factory, Addis Ababa, Ethiopia. The dye's characteristics and structure are illustrated in Table 1 and Figure 1, respectively. A 1,000 mg/L stock dye solution was prepared using distilled water and diluted as necessary to obtain dye solutions required for batch experiments.

Table 1 | Characteristics of RR198

Characteristic	RR198
Molecular formula	$C_{27}H_{18}C_lN_7Na_4O_{15}S_5$
Color index name	Reactive Red-198
λmax	520 nm
Molecular weight	967.5 g/mol

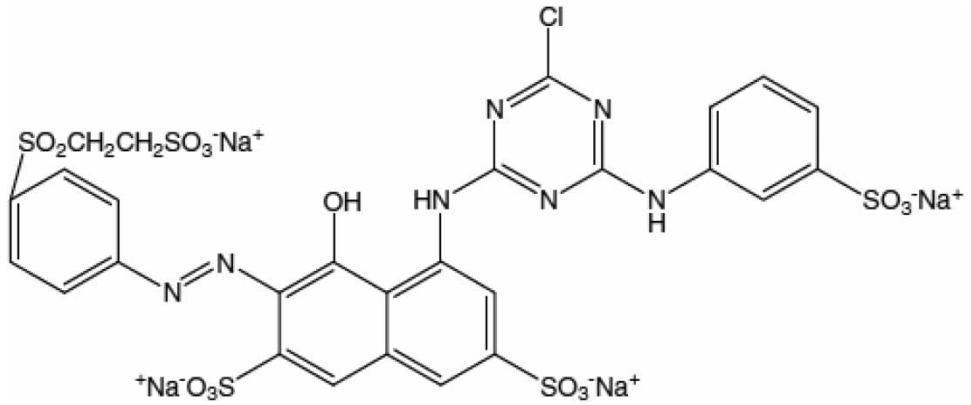

Figure 1 | Chemical structure of RR198 (Alimohammadi *et al.* 2016).

2.2. Adsorbent characterization

Scanning electron microscopy (SEM) (INSPECT, F50, USA) was used to examine the surface morphology of adsorbent materials. Fourier transform infrared spectroscopy (FTIR) (Perkin Elmer, USA) was used to analyze the adsorbents' functional groups. Infrared spectra were recorded in the 4,000–400 cm^{-1} region at 4 cm^{-1} resolution. Brannuer-Emmett-Teller (BET) (SA-9600 series, Japan) was used to determine raw adsorbent specific surfaces. The structure of the crystalline phases of the bentonite and SCBA were identified using XRD (XRD-7000, Japan). UV A spectrophotometer (JASCO V-770) was used to determine the concentration of RR198 in the solution by recording the UV absorbance at λmax 520 nm.

2.3. Batch experiments

The effect on adsorption of parameters such as solution pH (2 to 12), contact time (0 to 240 minutes), adsorbent dosage (0.5 to 3 g/L), and initial dye concentration (15 to 100 mg/L) were investigated. Batch experiments were carried at 25 °C using a magnetic stirrer at 200 rpm. The desired quantity of the blended adsorbents was added in 250 mL Erlenmeyer flasks (working volume 200 mL) containing 50 mg-RR198/L. The solution pH was adjusted by adding 0.1M HCl or NaOH. After mixing for a given contact time, the mixture was filtered using Whitman filter paper (185 mm diameter Cat No 1004 185) and the filtrate analyzed. An adsorbent recycling study was also carried out.

The absorbance concentration profile was obtained by plotting the dye absorbance calibration curve from the dye absorbance and concentrations graph. The absorbance for each sample was converted to the final dye concentration using the calibration factor obtained from the calibration curve. The amount of dye adsorbed on the adsorbent surface at time (t) can be calculated from the mass balance Equation (1).

$$q_t = (C_o - C_t)\frac{V}{m} \tag{1}$$

where, q_t is the amount of dye adsorbed per unit mass of adsorbent (mg/g), C_o the initial dye concentration (mg/L), C_t the equilibrium dye concentration (mg/L), V the dye solution volume (mL), and m the adsorbent mass (g).

Proportional dye removal (%) was calculated using Equation (2).

$$\text{Proportional dye removal (\%)} = \frac{(C_o - C_t)}{C_o} * 100 \tag{2}$$

2.4. Kinetic study

Three known established kinetic models – the pseudo-first-order (PFO), pseudo-second-order (PSO) and intraparticle diffusion (ID) models – were chosen to analyze adsorption capacity at different contact times and reaction rate constants involved during adsorption.

All of the models were determined according to linear Equations (3)–(5) (Alemayehu *et al.* 2011; Singh *et al.* 2020).

$$\log(q_e - q_t) = \log(q_e) - \frac{K_1 t}{2.303} \tag{3}$$

$$\frac{t}{q_t} = \left(\frac{1}{q_e}\right)t + \frac{1}{K_2 q_e^2} \tag{4}$$

$$\log(q_t) = \log(K_p) + 0.5\log(t) \tag{5}$$

where, q_e is the mass of dye adsorbed at equilibrium (mg/g), q_t the mass of dye adsorbed at time t (mg/g), K_1 the PFO constant (min^{-1}), K_2 the PSO constant (g/mg/min), and K_p the ID constant ($mg/g/min^{0.5}$).

2.5. Adsorption isotherms

The Langmuir and Freundlich adsorption isotherm linear models were used to analyze adsorbate/adsorbent interaction at equilibrium. The Langmuir isotherm model is used to establish the relationship in monolayer coverage of adsorbate molecules and homogeneous active sites on the adsorbent surface, and that there are no

interactions between adsorbed species (Dehvari *et al.* 2017). The assumption underlying the Freundlich model is that adsorption is onto a heterogeneous adsorbent. The Langmuir linear equation model (Carvalho *et al.* 2019) was evaluated using Equation (6) and the Freundlich linear equation model (Das *et al.* 2020a) using Equation (7).

$$\frac{C_e}{q_e} = \frac{1}{b.q_{\max}} + \frac{C_e}{q_{\max}} \tag{6}$$

$$\log q_e = \log K + \frac{1}{n}\log C_e \tag{7}$$

where, q_e is the specific amount of dye adsorbed (mg/g) and C_e the dye concentration in the liquid phase at equilibrium (mg/L). The Langmuir parameters are q_{max} (mg/kg), which is related to adsorption density, and b (L/mg), which indicates the adsorption energy. Both are calculated from the plot $1/q_e$ *vs* $1/C_e$.

The parameters K (L/kg) and n (dimensionless) are the Freundlich constants, and are related to the total adsorption capacity and intensity of adsorption, respectively. The Freundlich constant K_f is used to evaluate the relative capacity or power of adsorption of an adsorbent.

2.6. Data optimization model

Central composite design (CCD) is commonly applied under response surface methodology (RSM) to analyze experimental data. CCD was used to analyze the data obtained. Stat-Ease version 11 (Design Expert, USA) was used for the data processing. Table 2 shows three independent parameters: contact time, adsorbent dose, and initial dye concentration. The 3D plots and predicted vs. actual values were evaluated to interpret the interaction between the independent parameters, and their impact on the adsorption process. The general formula of the second-order mathematical model with interactions according to the dependent variable (y_i) in the response surface analysis (Asaithambi *et al.* 2017) is

$$yi = bo + \sum_{i=1}^{n} bixi + \sum_{i=1}^{n} biixi^2 + \sum_{j=i+1}^{n} bijxixj \tag{8}$$

where, y_i is the dye removal value, b_0 the constant coefficient, b_i (i = 1,2 and 3) the linear coefficients, b_{ii} (i = 1,2 and 3) the quadratic coefficients, b_{ij} (i = 1,2, and 3; j = 1,2 and 3) the interaction coefficients and x_i, x_j the coded factor values.

Table 2 | Independent variables and levels

	Range and levels				
Independent variables	**−1**	**0**	**+1**	**-α**	**+α**
Contact time (min)	30	105	180	21	231
Adsorbent dose (g)	0.5	1.75	3	0.35	3.8
Initial dye concentration (mg/L)	15	57.5	100	14	129

2.7. Desorption experiments

Desorption was done to enable adsorbent recycling and reuse multiple times, which will reduce costs (Muralikrishnan & Jodhi 2020). Before the desorption experiments, 3 g of bentonite blended with SCBA was added to a 250 mL flask containing 200 mL of 30 mg-RR198/L solution at a pH 2 and 25 °C. The flask was shaken at 200 rpm for 120 minutes until adsorption reached equilibrium and the residual dye concentration determined. The separated residue was added to a 250 mL flask containing 100 ml of 1M NaOH, which was shaken at 100 rpm for 7 hours. The desorption capacity (q_e) and efficiency (Q) were calculated using Equations (9) and (10).

$$q_e = V\left(\frac{C_f}{M}\right) \tag{9}$$

where, q_e is the amount desorbed (mg/g), V the solvent solution volume (L), M the weight of spent adsorbent (g) and C_f the dye concentration in the desorbing solution (mg/L).

$$Q(\%) = \left(\frac{q_{e,desorption}}{q_{e,sorption}}\right) * 100 \tag{10}$$

3. RESULTS AND DISCUSSION

3.1. Characterization of adsorbents

The specific surfaces determined were 57.7 m^2/g for raw bentonite and 4.94 m^2/g for raw SCBA. Previous study reports for bentonite were 66.2 (Al-Essa 2018), 25.7 (Toor *et al.* 2015), and 13.9 m^2/g (Carvalho *et al.* 2019), and 1.5 m^2/g for raw SCBA (Farirai *et al.* 2020). The XRD results for bentonite and SCBA are shown in Figure 2(a) and 2(b) respectively. Strong peaks at $2\theta = 19.5°$, 26.5°, and 28.4° for bentonite and $2\theta = 21.7°$, 24.3°, and 28° for SCBA were found. The bentonite peaks at $2\theta = 26.5°$, 28.4°, and 35.2° show the presence of quartz, as do those at $2\theta = 24.3°$, 28° and 35.7° for SCBA.

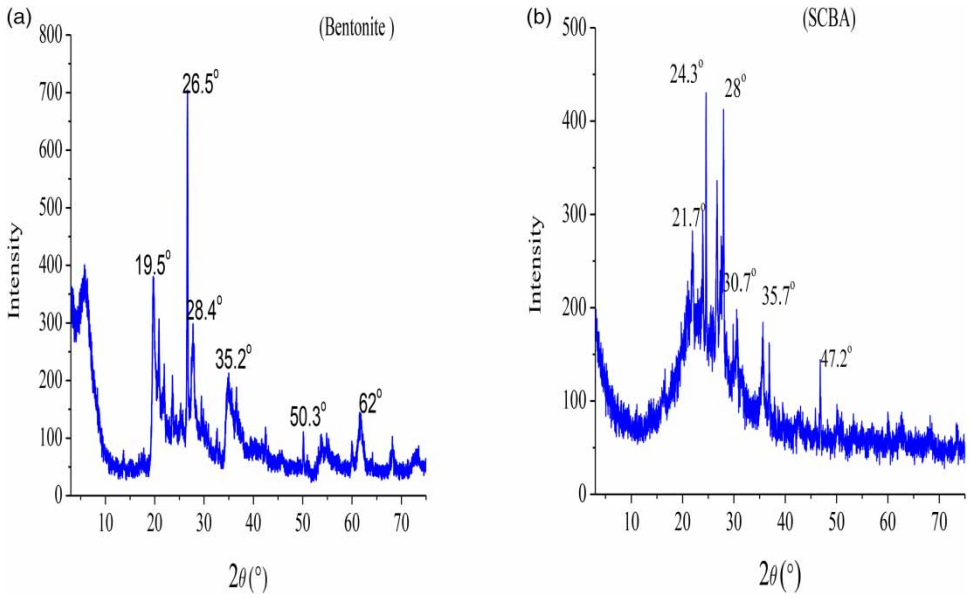

Figure 2 | XRD results for bentonite (a) and SCBA (b).

The FTIR results for both adsorbents are shown in Figure 3(a) and 3(b). The raw bentonite absorption band at 3,630 and 1,638 cm^{-1} indicates O-H group bending and stretching in the hydration water on the bentonite surface. Al-Essa (2018) observed peaks at 3,450 and 1,650 cm^{-1} indicating the presence of OH groups on the bentonite surface. Özcan & Özcan (2004) observed peaks at 3,446 and 3,629 cm^{-1}, because of OH group stretching bands. While the band at 1,640 cm^{-1}corresponds to OH group deformation on natural bentonite.

The very strong absorption band at 1,009 cm^{-1} is recognized as representing Si-O band stretching vibration, providing strong evidence for the presence of a silicate structure. The peaks at 779 and 507 cm^{-1} show the presence of quartz in the bentonite. Zhirong *et al.* (2011) report that the band at 796 cm^{-1} confirms the presence of quartz.

The FTIR analysis of SCBA shows a peak at 3,315 cm^{-1} representing the presence of OH on the ash surface. The peaks at 847, 784, and 422 cm^{-1} are due to Si-O-M (metal impurity) bonding, Al-O-Si bending vibrations, Si-O-Al deformation, and Si-O stretching, indicating the presence of crystalline quartz. The absorption band at approximately 770 to 797 cm^{-1} is caused by Si–O–Si symmetric stretching (Rahman *et al.* 2015).

Figure 4(a) and 4(b) show the surface morphology of raw bentonite and SCBA before adsorption and Figure 4(c) after adsorption. The SEM images in Figure 4(a) and 4(b) show that both adsorbents are rough and dense before adsorption, with pores and active sites available; the internal surface can also be seen. This confirms

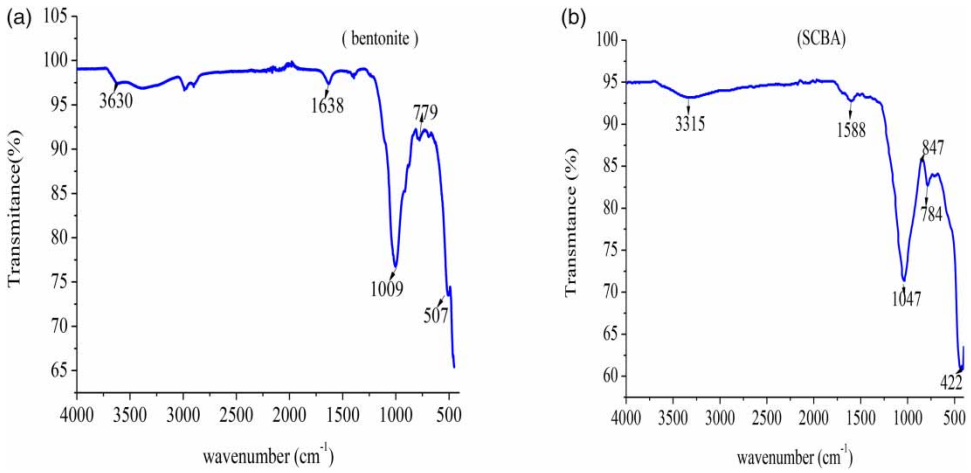

Figure 3 | FTIR results for bentonite (a) and SCBA (b).

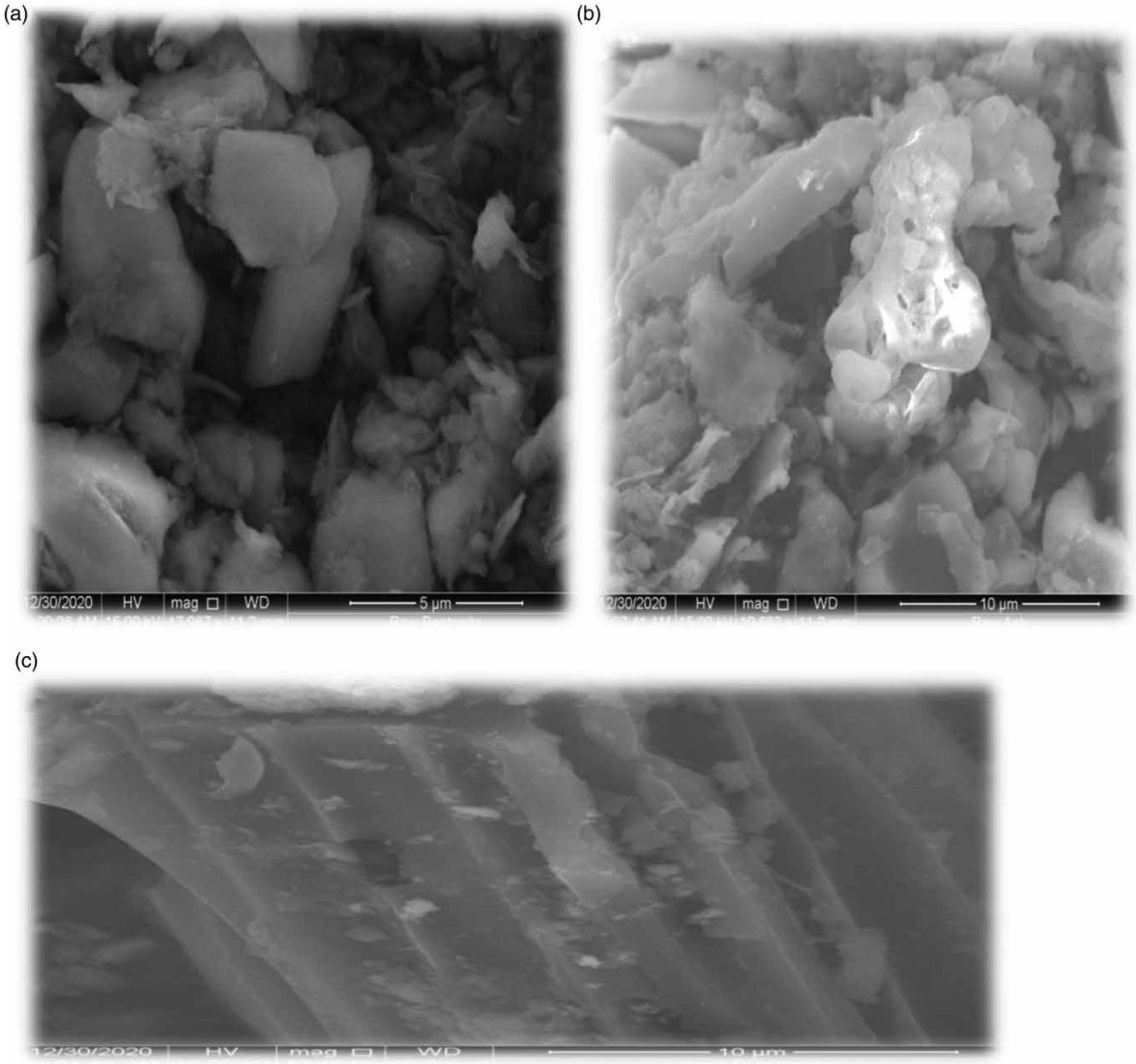

Figure 4 | SEM image of (a) unused bentonite, and (b) unused SCBA, and (c) mixed bentonite and SCBA after dye adsorption.

successful adsorbent formation, with homogeneous component dispersion and porous structures on the surfaces, which increase their dye sorption capacity. However, Figure 4(c) shows a rather smaller proportion of irregular structures, including pores, which can be attributed to dye adsorption on the adsorbent surfaces with active sites occupied. The surface texture of SCBA is similar to that observed by others (Alves *et al.* 2017; Farirai *et al.* 2020). The bentonite surface morphology is also similar to that reported by others (Javed *et al.* 2018; Carvalho *et al.* 2019).

3.2. Effect of pH

The solution pH is an essential factor in sorption because it can alter the adsorbate-adsorbent interaction surface charge, enhancing attraction or repulsion (Akar *et al.* 2018). In this study, the batch runs were carried out at various dye solution pH values (2, 4, 6, 8, 10, and 12) at 25 °C and stirred at 200 rpm. Figure 5 shows the impact of pH on RR198 sorption onto the blended adsorbents dosed at 2 g/L, initial dye (30 mg/L), and contact time 60 minutes. As can be seen, removal efficiency fell from 86 to 24% with increasing pH. The maximum dye removal efficiency and sorption ability were achieved at pH 2. Acidic conditions (low pH) enhance H^+ ion concentrations, which develop a positive surface charge by binding the H^+ ion onto the adsorbent surface. Negatively charged groups on the dye surface were attracted by the positive groups on the adsorbent surface (Alimohammadi *et al.* 2016). The effect of pH on the adsorption of reactive dyes such as reactive red 2, reactive orange and reactive blue 4, is to yield maximum removal efficiency at low values. For instance, when using coir pith as the adsorbent Çolak *et al.* (2009) and Salari *et al.* (2021) also reported the highest RR198 removal efficiency at pH 2.

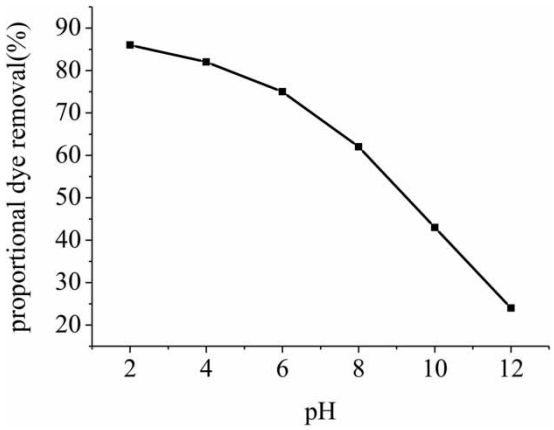

Figure 5 | Effect of pH on RR198 dye removal efficiency.

3.3. Effect of adsorbent dosage

A series of batch runs was carried out using different adsorbent doses; that is, 0.5, 1, 1.5, 2.5, and 3 g/L, other conditions remaining the same (stirred at 200 rpm, temperature 25 °C, contact time 60 minutes, initial dye concentration 70 mg/L, and solution pH 2). Figure 6 shows that as the adsorbent dose was increased from 0.5 to 3 g/L, the proportional amount of dye adsorbed (q_e) fell from 8.24 to 3.4 mg/g, while dye removal efficiency rose from 27.4 to 73%. Other studies have shown similar phenomena; for example, Carvalho *et al.* (2019) used activated carbon and bentonite to adsorb direct orange 39 dye, and Das *et al.* (2020b) removed malachite green dye using bio-degradable sodium alginate/NaOH-treated activated sugar cane bagasse charcoal. Increasing the adsorbent dose increases the number of active sites available (Dehvari *et al.* 2017).

3.4. Effect of initial dye concentration

A similar series of runs to those reported in sub-section 3.3 involved different initial dye concentrations; that is, 15, 30, 50, 70, and 100 mg/L, other conditions remaining the same, with contact time 150 minutes, adsorbent dose 3 g, and pH 2. Figure 7 shows the results. As can be seen, a higher initial dye concentration leads to a decrease in proportional dye removal. The amount of dye adsorbed increased from 0.89 mg/g at 15 mg/L initial dye concentration to 3.8 mg/g at 100 mg/L initial dye concentration, while proportional dye removal fell from 89% at 15 mg/L to 57% at 100 mg/L initial concentration. If active sites are available on the adsorbent surface, proportional dye removal

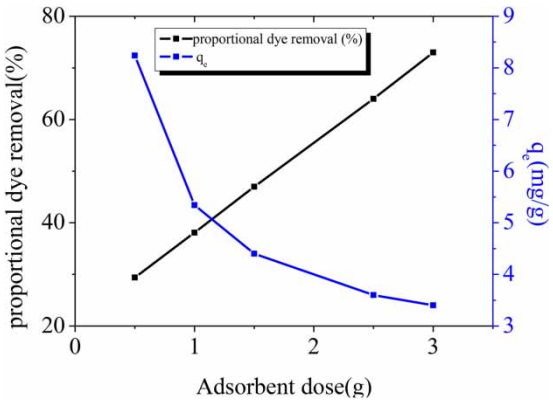

Figure 6 | Effects of adsorbent dose.

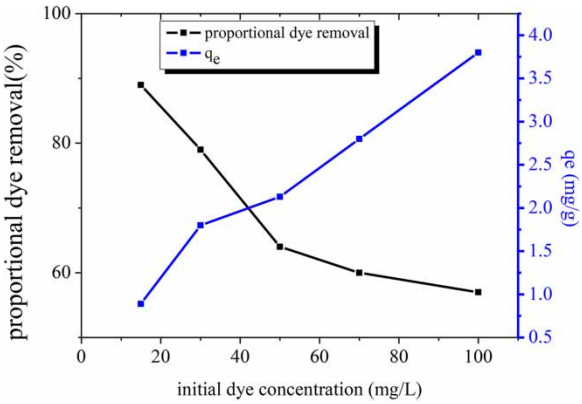

Figure 7 | Effect of initial dye concentration.

increases with increasing initial concentration, while, if active sites are saturated, proportional dye removal decreases (Zhou *et al.* 2019). Thus, the higher proportional dye removal at lower initial concentration can be attributed to increased probability of binding all dye molecules to vacant adsorbent sites. Mahanna & Samy (2020) reported similar results in reactive red 195 dye removal using acid-modified soybean leaves.

3.5. Effect of contact time

A further, similar set of batch experiments was carried out with different contact times; that is, 0, 30, 60, 90, 120, 150, 180, 210, and 240 minutes. All other factors were kept the same as noted above (sub-section 3.4). Figure 8 shows that dye removal began at some point within 50 minutes of start-up, and then proceeded at a fairly constant rate until almost reaching equilibrium after 150 minutes, after which removal efficiency decreased, perhaps because desorption occurred and active sites were occupied, leading to an increase in dye concentration in solution (Saha *et al.* 2012; Das *et al.* 2020b).

3.6. Adsorption kinetics

Table 3 shows that the PSO model fitted the trial results better than the other models, with $R^2 = 0.98$ indicating that chemical adsorption is more probable than physical adsorption. This is attributed to electron interaction between RR198 dye molecules and the blended bentonite and SCBA during chemical adsorption (Alimohammadi *et al.* 2016; Tayebi *et al.* 2016).

3.7. Isothermal study

The Langmuir isotherm model was evaluated using Equation (6), and constants q_{max} (mg/g) and b (L/g) were analyzed from the slope and intercept of C_e/q_e vs C_e respectively. The dye concentration range was from 15 to 100 mg/L, but no other factors changed. The values of q_{max} and b were 4.24 mg/g and 0.097 L/g. The Freundlich isotherm model was analyzed using Equation (7), and the constant values K and n were evaluated from the

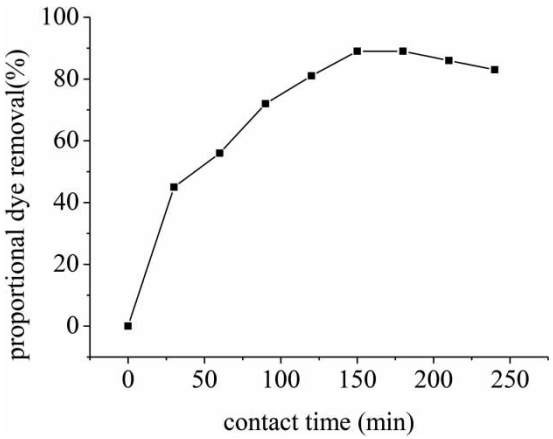

Figure 8 | Effect of contact time on dye removal efficiency.

Table 3 | Parameters obtained from PFO, PSO and ID models

	PFO			PSO			ID	
Model parameters	q_e	K_1	R^2	q_e	K_2	R^2	K_p	R^2
Values	1.8	0.007	0.63	3.36	0.009	0.98	0.525	0.88

intercept and slope of $\log q_e$ vs $\log C_e$ respectively. The calculated values of n and K were 2.4636 ($n > 1$) and 0.755 L/kg, indicating the greater favorability of the sorption process in the Freundlich than the Langmuir model. The sorption equilibrium result indicated the best fit for the Freundlich model ($R^2 = 0.95$), R^2 for the

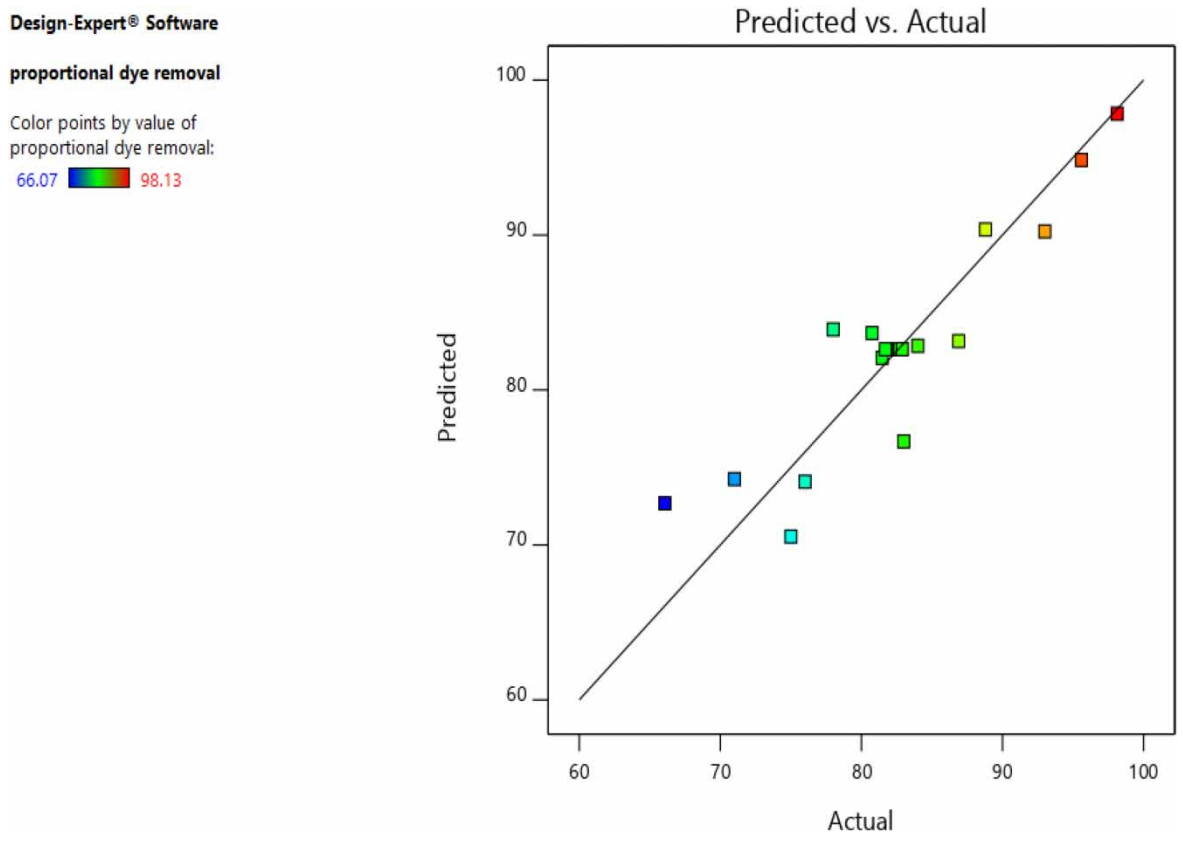

Figure 9 | Predicted vs actual RR198 dye removal on blended bentonite and SCBA.

Langmuir model was 0.87 (Table 4). This showed the heterogeneous distribution of binding sites on the surface of the blended adsorbents.

3.8. RSM results

The dye removal results were evaluated using RSM. Figure 9 shows that the actual and predicted dye removal efficiencies were close for the RR198 removal studies.

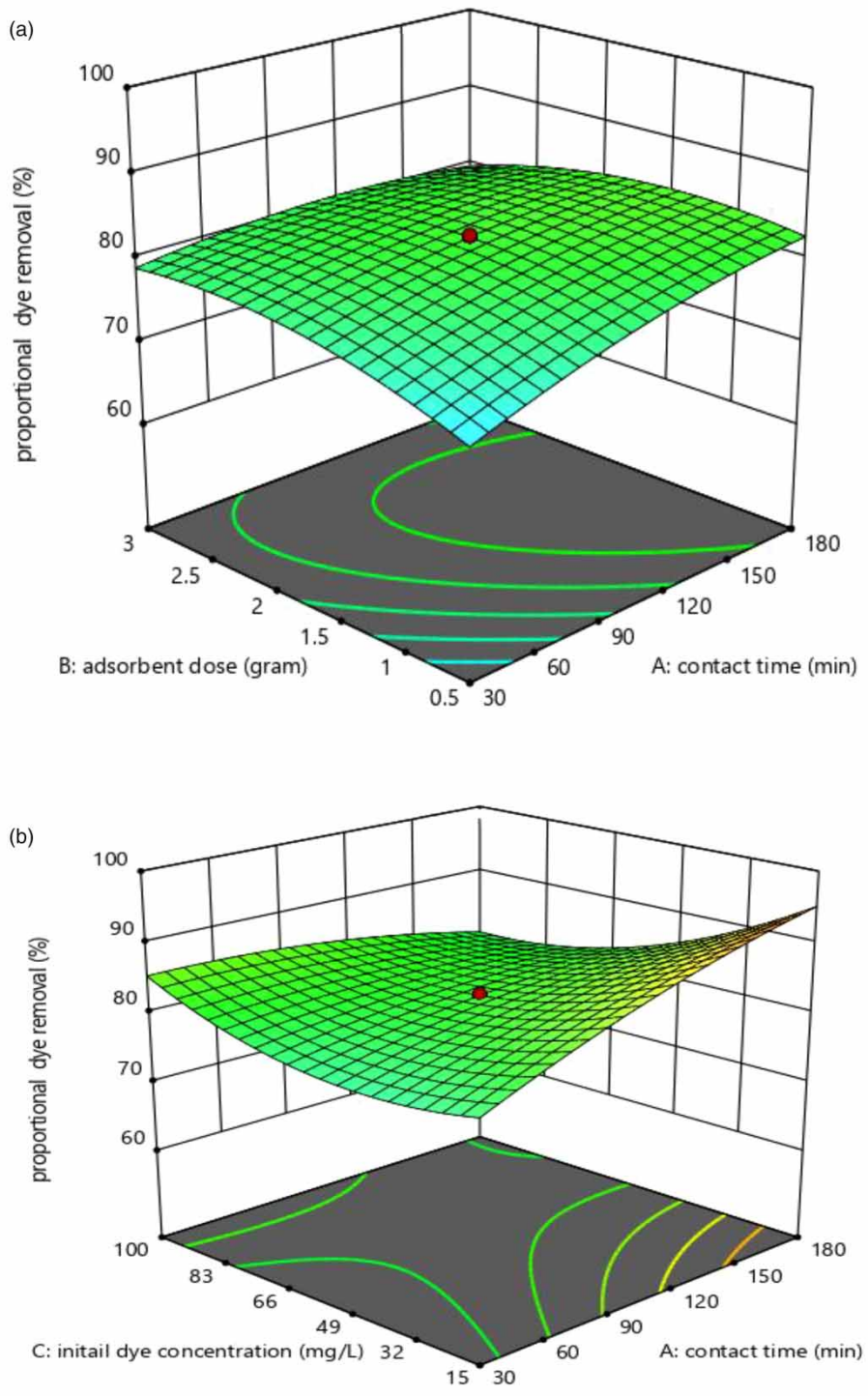

Figure 10 | 3D surface plots on the combined effects of (a) adsorbent dose and contact time, (b) initial concentration and contact time, and (c) adsorbent dose and initial concentration.

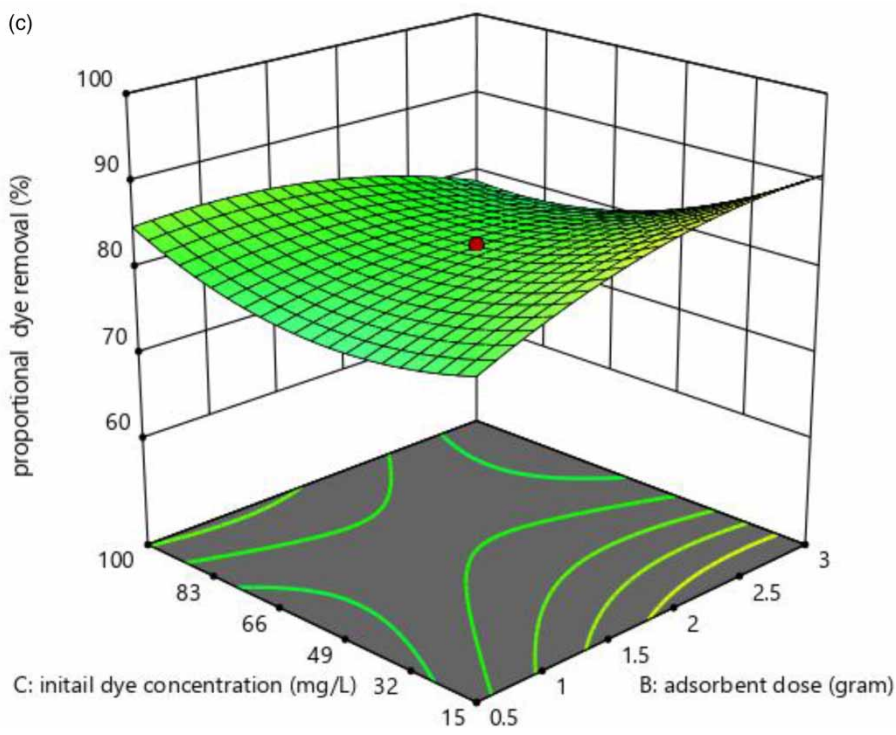

Figure 10 | Continued.

3.8.1. Effect of adsorbent dose vs contact time

Figure 10(a) shows that proportional dye removal increased with increasing adsorbent dose and contact time, and that the maximum adsorption of 82.9% was achieved with an adsorbent dose of 1.75 g/L and contact time 105 minutes. This arose because of the number of vacant active adsorbing sites and the availability of enough time for adsorbent-adsorbate contact (Igwegbe *et al*. 2019; Das *et al*. 2020a).

3.8.2. Effect of contact time vs initial concentration

The interactive effect of contact time and initial adsorbate concentration on RR198 removal efficiency is illustrated in the 3D graph in Figure 10(b). This shows that RR198 removal efficiency increased with increasing contact time. The maximum calculated adsorption efficiency was 93.2%, at 197 minutes contact time and just under 19 mg/L initial dye concentration. The interaction model results indicate that adsorption efficiency was higher with longer contact time because enough time is available for interaction between dye molecules and the adsorbent surface (Brahmi *et al.* 2019).

3.8.3. Effect of adsorbent dose vs initial dye concentration

Figure 10(c) illustrates the interactive effect of adsorbent dose and initial dye concentration on RR198 removal. As can be seen, raising the adsorbent dose from 0.5 to 3 g/L increased dye removal efficiency, while the increase in initial dye concentration reduced efficiency. The highest proportional dye removal was achieved at low initial dye concentration and high adsorbent dose, and the optimal result was 90.7% dye removal efficiency at a bit more than 15 mg/L initial dye concentration and 2.9 g/L blended adsorbent dose. The adsorbent dose increase enhanced the availability of free active sites on the adsorbent surface (Saha *et al*. 2012; Davarnejad *et al.* 2020). This may occur because of the reduced ratio of active sites to dye molecules, so that there was insufficient vacant space on the adsorbent surface (Brahmi *et al.* 2019).

3.9. Desorption and reusability experiment

Figure 11 shows the blended adsorbent's removal efficiency through three cycles of desorption-adsorption. As can be seen, the proportional removal performance fell from 86 to 84.2% between the first and third cycles. At the same time, the adsorption capacity also fell from 2.6 to 2.3 mg/g. These results confirm that bentonite blended with SCBA can be reused for RR198 removal from wastewaters.

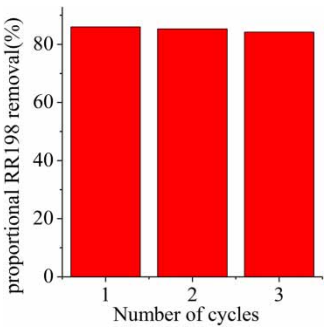

Figure 11 | Number of cycles vs adsorption efficiency.

Table 4 | Isotherm models for RR198 dye adsorption onto blended bentonite and SCBA

	Langmuir			Freundlich		
Isotherm parameters	**q_{max}**	**b**	**R^2**	**n**	**K**	**R^2**
Values	4.24	0.097	0.87	2.4636	0.755	0.95

4. CONCLUDING REMARKS

RR198 adsorption was investigated using bentonite blended with SCBA as the adsorbent. The adsorption isotherm model was fitted better by Freundlich than Langmuir, while the pseudo-second-order model fitted the adsorption kinetics best. CCD under RSM was used to investigate the interaction between contact time, adsorbent dose, and initial dye concentration – three independent parameters – on RR198 adsorption. Use of RSM enabled determination of the optimal parameters for removal of the dye, and the precise values of 107 minutes contact time, 0.934 g adsorbent dose, and 15 mg/L initial dye concentration were found to give 85.2% RR198 dye removal efficiency. Desorption and reusability studies were carried out in batch mode and confirmed that bentonite blended with SCBA can be used multiple times for dye removal from aqueous solution. In general, the results indicated that natural bentonite blended with sugar cane bagasse ash can be used to treat textile industry wastewaters to remove RR198 dyes. The blend is an efficient and environment-friendly adsorbent.

ACKNOWLEDGEMENTS

This work was funded by Addis Ababa Science and Technology University and *Debre Tabor* University. The authors would like to thank the Environmental Engineering Department of Addis Ababa Science and Technology University, for offering complete laboratory facilities, *Yirgalem* Addis Textile factory for providing reactive dyes, *Wonji Shewa* sugar factory for providing sugar cane bagasse ash and *Candela* pharmaceutical industry for supporting FTIR instrument analysis of functional sample groups.

DECLARATION

We declare that there is no conflict of interest.

DATA AVAILABILITY STATEMENT

All relevant data are included in the paper or its Supplementary Information.

REFERENCES

Adebayo, M. A., Adebomi, J. I., Abe, T. O. & Areo, F. I. 2020 Removal of aqueous Congo red and malachite green using ackee apple seed – bentonite composite. *Colloid and Interface Science Communications* **38**, 100311. Elsevier, Amsterdam, the Netherlands.

Akar, T., Uzun, C., Çelik, S. & Akar, S. T. 2018 Biosorption of basic blue 7 by fungal cells immobilized on the Green-type biomatrix of *Phragmites australis* spongy tissue. *International Journal of Phytoremediation* **20**(2), 145–152.

Alemayehu, E., Thiele-Bruhn, S. & Lennartz, B. 2011 Adsorption behaviour of Cr(VI) onto macro and micro-vesicular volcanic rocks from water. *Separation and Purification Technology* **78**(1), 55–61.

Al-Essa, K. 2018 Activation of Jordanian bentonite by hydrochloric acid and its potential for olive mill wastewater enhanced treatment. *Journal of Chemistry* **2018**, 8385692.

Alimohammadi, Z., Younesi, H. & Bahramifar, N. 2016 Batch and column adsorption of reactive red 198 from textile industry effluent by microporous activated carbon developed from walnut shells. *Waste and Biomass Valorization* **7**(5), 1255–1270. Springer, Berlin/Heidelberg.

Alves, R. H., Reis, T. V. D. S., Rovani, S. & Fungaro, D. A. 2017 Green synthesis and characterization of biosilica produced from sugarcane waste ash. *Journal of Chemistry* **2017**, 6129035.

Asaithambi, P., Alemayehu, E., Sajjadi, B., Raman, A. & Aziz, A. 2017 Electrical energy per order determination for the removal pollutant from industrial wastewater using UV/Fe_{2+}/H_2O_2 process: optimization by response surface methodology. *Water Resources and Industry* **18**, 17–32. Elsevier, Amsterdam, the Netherlands.

Brahmi, L., Kaouah, F., Boumaza, S. & Trari, M. 2019 Response surface methodology for the optimization of acid dye adsorption onto activated carbon prepared from wild date stones. *Applied Water Science* **9**(8), 1–13. Springer International Publishing, Berlin/Heidelberg.

Carvalho, L. A. S. J., Konzen, R. A., Cunha, A. C. M., Batista, P. R., Bassetti, F. J. & Coral, L. A. 2019 Efficiency of activated carbons and natural bentonite to remove Direct orange 39 from water. *Journal of Environmental Chemical Engineering* **7**(6), 103496. Elsevier, Amsterdam, the Netherlands.

Çolak, F., Atar, N. & Olgun, A. 2009 Biosorption of acidic dyes from aqueous solution by *Paenibacillus macerans*: kinetic, thermodynamic and equilibrium studies. *Chemical Engineering Journal* **150**(1), 122–130.

Das, L., Das, P., Bhowal, A. & Bhattachariee, C. 2020a Synthesis of hybrid hydrogel nano-polymer composite using Graphene oxide, Chitosan and PVA and its application in waste water treatment. *Environmental Technology and Innovation* **18**, 100664. Elsevier, Amsterdam, the Netherlands.

Das, L., Das, P., Bhowal, A. & Bhattachariee, C. 2020b Treatment of malachite Green dye containing solution using bio-degradable sodium alginate/NaOH treated activated sugarcane bagasse charcoal beads: batch, optimization using response surface methodology and continuous fixed bed column study. *Journal of Environmental Management* **276**, 111272. Elsevier, Amsterdam, the Netherlands.

Davarnejad, R., Afshar, S. & Etehadfar, P. 2020 Activated carbon blended with grape stalks powder: properties modification and its application in a dye adsorption. *Arabian Journal of Chemistry* **13**(5), 5463–5473.

Dawood, S. & Sen, T. K. 2012 Removal of anionic dye Congo red from aqueous solution by raw pine and acid-treated pine cone powder as adsorbent: equilibrium, thermodynamic, kinetics, mechanism and process design. *Water Research* **46**(6), 1933–1946. Elsevier, Amsterdam, the Netherlands.

Dehvari, M., Ehrampoush, M. H., Ghaneian, M. T., Jamshidi, B. & Tabatabaee, M. 2017 Adsorption kinetics and equilibrium studies of reactive red 198 dye by cuttlefish bone powder. *Iranian Journal of Chemistry and Chemical Engineering* **36**(2), 143–151.

Dizge, N., Aydiner, C., Demirbas, E., Kobya, M. & Kara, S. 2008 Adsorption of reactive dyes from aqueous solutions by fly ash: kinetic and equilibrium studies. *Journal of Hazardous Materials* **150**(3), 737–746.

Farirai, F., Mupa, M. & Daramola, M. O. 2020 An improved method for the production of high purity silica from sugarcane bagasse ash obtained from a bioethanol plant boiler. *Particulate Science and Technology* **39**(2), 1–8.

Garg, V. K., Gupta, R., Yadav, A. B. & Kumar, R. 2003 Dye removal from aqueous solution by adsorption on treated sawdust. *Bioresource Technology* **89**(2), 121–124.

Gupta, V. K., Mittal, A., Krishnan, L. & Gajbe, V. 2004 Adsorption kinetics and column operations for the removal and recovery of malachite Green from wastewater using bottom ash. *Separation and Purification Technology* **40**(1), 87–96.

Huabcharoen, P., Wimolmala, E., Markpin, T. & Sombatsompop, N. 2017 Purification and characterization of silica from sugarcane bagasse ash as a reinforcing filler in natural rubber composites. *BioResources* **12**(1), 1228–1245.

Igwegbe, C. A., Mohmmadi, L., Ahmadi, S., Rahdar, A., Khadkhodaiy, D., Dehghani, R. & Rahdar, S. 2019 Modeling of adsorption of methylene blue dye on Ho-$CaWO_4$ nanoparticles using response surface methodology (RSM) and artificial neural network (ANN) techniques. *MethodsX* **6**, 1779–1797. Elsevier, Amsterdam, the Netherlands.

Jain, S. N. & Gogate, P. R. 2018 Efficient removal of acid Green 25 dye from wastewater using activated *Prunus dulcis* as biosorbent: batch and column studies. *Journal of Environmental Management* **210**, 226–238. Elsevier, Amsterdam, the Netherlands.

Javed, S. H., Zahir, A., Khan, A., Afzal, S. & Mansha, M. 2018 Adsorption of mordant Red 73 dye on acid activated bentonite: kinetics and thermodynamic study. *Journal of Molecular Liquids* **254**, 398–405. Elsevier, Amsterdam, the Netherlands.

Khalilzadeh Shirazi, E., Metzger, J. W., Fischer, K. & Hassani, A. H. 2020 Removal of textile dyes from single and binary component systems by Persian bentonite and a mixed adsorbent of bentonite/charred dolomite. *Colloids and Surfaces A: Physicochemical and Engineering Aspects* **598**, 124807. Elsevier, Amsterdam, the Netherlands.

Mahanna, H. & Samy, M. 2020 Adsorption of reactive red 195 dye from industrial wastewater by dried soybean leaves modified with acetic acid. *Desalination and Water Treatment* **178**, 312–321.

Mall, I. D., Srivastava, V. C., Agarwal, N. K. & Mishra, I. M. 2005 Removal of Congo red from aqueous solution by bagasse fly ash and activated carbon: kinetic study and equilibrium isotherm analyses. *Chemosphere* **61**(4), 492–501.

Moussavi, G. & Khosravi, R. 2011 The removal of cationic dyes from aqueous solutions by adsorption onto pistachio hull waste. *Chemical Engineering Research and Design* **89**(10), 2182–2189.

Muralikrishnan, R. & Jodhi, C. 2020 Biodecolorization of reactive dyes using biochar derived from coconut shell: batch, isotherm, kinetic and desorption studies. *ChemistrySelect* **16**, 7734–7742.

Özcan, A. S. & Özcan, A. 2004 Adsorption of acid dyes from aqueous solutions onto acid-activated bentonite. *Journal of Colloid and Interface Science* **276**(1), 39–46.

Pandey, S. & Ramontja, J. 2016 Natural bentonite clay and its composites for dye removal: current state and future potential. *American Journal of Chemistry and Applications* **3**(2), 8–19.

Rahman, N. A., Widhiana, I., Juliastuti, S. R. & Setyawan, H. 2015 Synthesis of mesoporous silica with controlled pore structure from bagasse ash as a silica source. *Colloids and Surfaces A: Physicochemical and Engineering Aspects* **476**, 1–7. Elsevier, Amsterdam, the Netherlands.

Saha, P. D., Chowdhury, S., Mondal, M. & Sinha, K. 2012 Biosorption of direct Red 28 (Congo Red) from aqueous solutions by eggshells: batch and column studies. *Separation Science and Technology* **47**(1), 112–123.

Salari, N., Tehrani, R. M. A. & Motamedi, M. 2021 Zeolite modification with cellulose nanofiber/magnetic nanoparticles for the elimination of reactive red 198. *International Journal of Biological Macromolecules* **176**, 342–351.

Singh, R., Singh, T. S., Odiyo, J. O., Smith, J. A. & Edokpayi, J. N. 2020 Evaluation of methylene blue sorption onto low-cost biosorbents: equilibrium, kinetics, and thermodynamics. *Journal of Chemistry* **2020**, 8318049.

Song, K., Xu, H., Xu, L., Xie, K. & Yang, Y. 2017 Cellulose nanocrystal-reinforced keratin bioadsorbent for effective removal of dyes from aqueous solution. *Bioresource Technology* **232**, 254–262. Elsevier, Amsterdam, the Netherlands.

Srivastava, V. C., Mall, I. D. & Mishra, I. M. 2007 Adsorption thermodynamics and isosteric heat of adsorption of toxic metal ions onto bagasse fly ash (BFA) and rice husk ash (RHA). *Chemical Engineering Journal* **132**(1–3), 267–278.

Tayebi, H. A., Dalirandeh, Z., Shokuhi Rad, A., Mirabi, A. & Binaeian, E. 2016 Synthesis of polyaniline/Fe_3O_4 magnetic nanoparticles for removal of reactive red 198 from textile waste water: kinetic, isotherm, and thermodynamic studies. *Desalination and Water Treatment* **57**(47), 22551–22563.

Toor, M., Jin, B., Dai, S. & Vimonses, V. 2015 Activating natural bentonite as a cost-effective adsorbent for removal of Congo-red in wastewater. *Journal of Industrial and Engineering Chemistry* **21**, 653–661.

Zhirong, L., Azhar Uddin, M. & Zhanxue, S. 2011 FT-IR and XRD analysis of natural Na-bentonite and Cu(II)-loaded Na-bentonite. *Spectrochimica Acta – Part A: Molecular and Biomolecular Spectroscopy* **79**(5), 1013–1016. Elsevier, Amsterdam, the Netherlands.

Zhou, Y., Zhang, L. & Cheng, Z. 2015 Removal of organic pollutants from aqueous solution using agricultural wastes: a review. *Journal of Molecular Liquids* **212**, 739–762. Elsevier, Amsterdam, the Netherlands.

Zhou, Y., Lu, J., Zhou, Y. & Liu, Y. 2019 Recent advances for dyes removal using novel adsorbents: a review. *Environmental Pollution* **252**, 352–365. Elsevier, Amsterdam, the Netherlands.

First received 22 October 2021; accepted in revised form 12 December 2021. Available online 24 December 2021